

To the associate editor,

Regarding the submitted manuscript (bg-2018-85), this document contains the following:

1. A point by point response to the reviewer's comments
2. A version of the manuscript highlighting all the changes from the previous version.

Finally, here is a brief list of relevant changes.

1. Storage fluxes have been incorporated into the estimation of OCS flux.
2. Inferences about soil moisture have been changed in accordance with reviewer comments.
3. Box plots have been added to Fig. 7 to help visualize the difference between fluxes observed during heat wave events.

On behalf of all the co-authors, I look forward to hearing from you.

Sincerely,
Bharat Rastogi
30 October, 2018

GENERAL COMMENTS

The authors have done a nice job improving this manuscript, which is more clear and reads well. I have just a few concerns remaining, noted below. With these addressed, I think the paper will make an important contribution to the literature.

We thank the reviewer for providing another round of detailed and valuable comments to help us improve the manuscript. Please see our responses to each comment below.

SPECIFIC COMMENTS

(1) Regarding the OCS flux estimation (Section 2.8)...

First, in the context of flux-gradient theory, g is the conventional symbol for conductance and I think it should not be used for “gradient”.

We agree and have changed the symbol for gradient to delta (Δ).

Second, I would spell out the theoretical idea a little more accurately in Section 2.8, as it differs significantly from the Commane et al 2015 paper that is cited as its basis. In Commane et al 2015, the flux-gradient approach was applied to turbulent flux; the assumption was that the turbulent conductance ($g = F/\text{gradient}$) for all gases was the same (no normalization for relative diffusivities necessary because turbulent flux is not diffusive), so that the gradients of the two gases (along a wholly above-canopy turbulent path that passed no sources or sinks) and the flux of one could be used to calculate the flux of the other. Here, instead, your gradient is between the inside of the leaf and the canopy-top atmosphere, which is a path that is mostly diffusive (stomata and, partially, the leaf boundary layer) but partly turbulent (the within-canopy airspace and, partially, the leaf boundary layer), and which may include unaccounted-for sources/sinks in the form of storage flux (i.e. changes in the canopy airspace concentrations) and lateral advection. By normalizing by the diffusivity ratio (i.e. treating the whole path as diffusive) and by neglecting storage and advection, you are effectively taking your canopy-top measurements to represent leaf surface measurements and your eddy flux to represent flux through the stomata. That will definitely invoke some error (possibly bias) and may or may not be a sufficient approximation, so I think the paper should discuss these assumptions and approximations that you are making, how they differ from the cited works, and the resulting uncertainty in the results (ideally quantitatively).

In your response to the first-round review, you argued: “In tall canopies such as our site, the portion of canopy that is coupled to the overlying atmosphere changes considerably during the

day, and parts of the lower canopy are likely to be always decoupled from the upper canopy as well as above canopy air (Pyles et al., 2004). This has obvious consequences on canopy storage and venting of gases such as CO₂ and OCS.” I agree, and this is exactly why taking canopy-top concentrations and fluxes to represent leaf-surface concentrations and fluxes will invoke error. It is also exactly why storage should be accounted for (not neglected, as you argued). If a significant portion of the flux through the stomata is going into (or coming from) changes in canopy concentration, then your flux gradient equations will become significantly inaccurate.

We thank you for this careful and detailed explanation regarding the turbulent and diffusive modes of resistance to flow of gases between the bulk atmosphere and inside the leaves. We showed in our earlier response that at this needle-leaf forest, stomatal (i.e. diffusive) resistance was by far the chief resistance to flow. You are absolutely correct about missing sources/sinks by not accounting for storage fluxes. However, there is considerable uncertainty in the estimation of storage flux, related to the averaging time and vertical resolution of the storage profile (Yang et al., 2007) as well as horizontal resolution (de Araújo et al., 2010; Nicolini et al., 2018). This is especially true at our site, where storage estimates can vary tremendously depending on how this term is estimated. Three different estimates of storage flux are shown (Fig. 1), as estimated from profile measurements. The first is using discrete measurements at the reference height (S₇₀), the second is by using measurements along the entire profile (S₇₀₋₁), and finally one using only the two heights at the canopy top (S₇₀₋₆₀). Importantly, over the course of the average day, each flux cumulatively sums up to zero. At Wind River, storage fluxes for CO₂ have been estimated using a discrete measurement only at the reference height (Falk et al., 2008). However, this results in a flux that is not significantly different from 0, which we know is incorrect. If instead, the entire profile is used, the mid-morning storage flux exceeds inferred GPP and is over twice the estimated turbulent flux. This is also likely incorrect, given that wind speed is usually high at 70m and the needle-leaf canopy top is well coupled to the overlying atmosphere. However, the understory at the site is decoupled from the overstory at all times of day, and movement of air in the sub-canopy is controlled by topographically generated (mountain/valley) katabatic flows; this is understandable due to the tall and dense canopy. Thus, turbulent fluxes measured by EC are principally influenced by the upper canopy layers. Incorporating measurements of the decoupled understory can account for large errors in flux estimation (e.g. Jocher et al., 2018). Given the within-canopy decoupling we use estimated storage flux based only on the top two measurement heights (i.e., use the 70m and 60m inlets), allowing us to incorporate the effect of change in storage on the estimation of an ecosystem OCS flux that is predominantly from the upper canopy

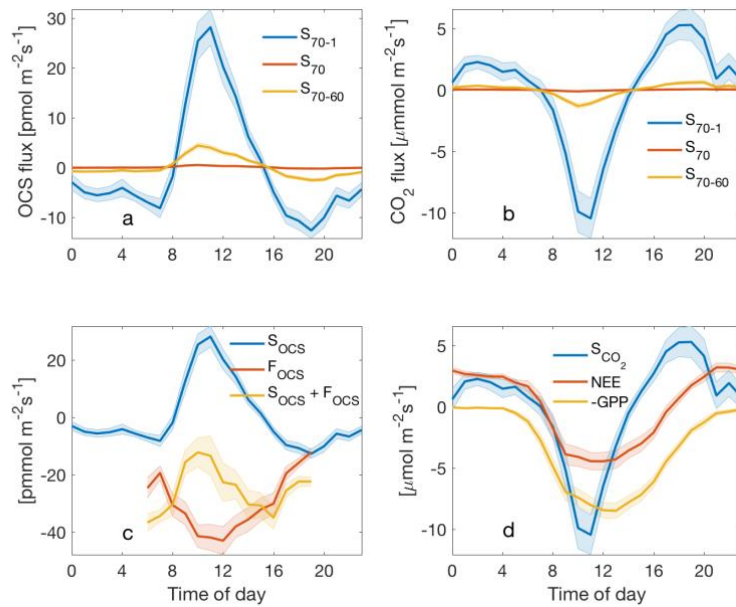


Figure 1. Mean diurnal cycles of OCS and CO₂ storage flux estimated using three different methods (a-b), and the storage flux estimated using the entire profile (S_{70-1}) compared to the NEE turbulent flux and the derived GPP (c-d).

(2) Regarding the response to heat waves (Section 3.5 and lines 462-464)...

This draft is better in that unsupported claims have been removed; however, the trade-off is that there doesn't seem to be a proper conclusion from the heat wave analysis. The only one offered is in the Conclusion section, which says that "sequential heatwaves lead to suppression in stomatal gas exchange of all three fluxes" — but that is not quite true, as F_{H_2O} is enhanced during the heatwaves. Moreover, the reduction of F_{OCS} is not so clear for the first two heat waves in Fig. 7, probably just due to the noise. Perhaps a regression plot or even just a simple statistic on heat-wave vs not-heat-wave F_{OCS} would help support the point that F_{OCS} , in keeping with GPP and G_c , is suppressed during heat waves.

We have added boxplots that show that during these heatwaves OCS uptake and canopy conductance are reduced, NEE is more positive, while F_{H_2O} fluxes are not significantly different. We have also added means for F_{OCS} in the text (line 453) that show the difference in these fluxes, and changed a line in the conclusion section (line 492) to say while F_{CO_2} and F_{OCS} are suppressed, F_{H_2O} is not.

(3) Regarding the influence of soil moisture...

I still do not see how the data support the inference that soil moisture (rather than a combination of VPD, temperature, and light) is driving seasonal changes in gas exchange, and although this draft backs away from strong statements about the soil moisture influence, it still suggests that soil moisture is a key driver in some places (e.g. abstract lines 28-29: "OCS fluxes

tracked changes in soil moisture”, and lines 411-413: “declining soil moisture likely limits gas exchange as the summer progresses, even as canopy conductance can be reasonably high under overcast skies”). Where soil moisture influence is suggested (and it is certainly a possibility that should be mentioned), it should be on par with other plausible explanations. It is probably also a good idea in general to note somewhere in the manuscript that it is not possible using the present data to tell the soil moisture influence apart from other factors. You attempt to disentangle the drivers in the discussion surrounding Fig 6, but I don’t follow the logic. I don’t see the Gc response being any more similar across time periods than the OCS or CO2 responses are, despite the text’s claim. Nor do I see why such an observation, if it were true, would implicate soil moisture as opposed to temperature or seasonal light levels.

We agree with the reviewer and have now removed soil moisture from the abstract (lines 29-29), and have changed lines 411-413 to say: “This indicates that declining soil moisture (Fig. 3b-c) potentially limits gas exchange as the summer progresses, even as canopy conductance can be reasonably high under overcast skies. It is important to note that in the absence of concurrent leaf and root water potential measurements, it is not possible to attribute reduction in gas exchange due to declining soil moisture.”

TECHNICAL CORRECTIONS

- line 235: Eq. 6 seems inverted. The correct equation is $\text{flux} = \text{conductance} \times \text{gradient} \Rightarrow \text{conductance} = \text{flux}/\text{gradient}$

Changed appropriately.

- lines 278-280: Fig 2 does not show the nighttime OCS flux.

We have removed these from the text

- Fig 2d: color scale should have a label (PAR).

Included in the current version.

- line 334: do you mean rainy days?

No. We have changed this to say decreased (line 343).

- line 376: “diffused: total” should be “diffuse:total” (no d and no space)

Changed appropriately.

References

de Araújo, A. C., Dolman, A. J., Waterloo, M. J., Gash, J. H. C., Kruijt, B., Zanchi, F. B., de Lange, J. M. E., Stoevelaar, R., Manzi, A. O., Nobre, A. D., Lootens, R. N. and Backer, J.: The spatial variability of CO₂ storage and the interpretation of eddy covariance fluxes in central Amazonia, *Agric. For. Meteorol.*, 150(2), 226–237, doi:10.1016/j.agrformet.2009.11.005, 2010.

Falk, M., Wharton, S., Schroeder, M., Ustin, S. and U, K. T. P.: Flux partitioning in an old-growth forest: seasonal and interannual dynamics, *Tree Physiol.*, 28(4), 509–520, 2008.

Jocher, G., Marshall, J., Nilsson, M. B., Linder, S., De Simon, G., Hörnlund, T., Lundmark, T., Näsholm, T., Ottosson Löfvenius, M., Tarvainen, L., Wallin, G. and Peichl, M.: Impact of Canopy Decoupling and Subcanopy Advection on the Annual Carbon Balance of a Boreal Scots Pine Forest as Derived From Eddy Covariance, *J. Geophys. Res. Biogeosciences*, 1–23, doi:10.1002/2017JG003988, 2018.

Nicolini, G., Aubinet, M., Feigenwinter, C., Heinesch, B., Lindroth, A., Mamadou, O., Moderow, U., Mölder, M., Montagnani, L., Rebmann, C. and Papale, D.: Impact of CO₂ storage flux sampling uncertainty on net ecosystem exchange measured by eddy covariance, *Agric. For. Meteorol.*, 248(September 2017), 228–239, doi:10.1016/j.agrformet.2017.09.025, 2018.

Yang, B., Hanson, P. J., Riggs, J. S., Pallardy, S. G., Heuer, M., Hosman, K. P., Meyers, T. P., Wullschleger, S. D. and Gu, L. H.: Biases of CO₂ storage in eddy flux measurements in a forest pertinent to vertical configurations of a profile system and CO₂ density averaging, *J. Geophys. Res. Atmos.*, 112(20), 1–15, doi:10.1029/2006JD008243, 2007.

1 **Ecosystem fluxes of carbonyl sulfide in an old-growth forest: temporal dynamics**
2 **and responses to diffuse radiation and heat waves**

3 Bharat Rastogi¹, Max Berkelhammer², Sonia Wharton³, Mary E Whelan⁴ Frederick C.
4 Meinzer⁵, David Noone⁶, and Christopher J. Still¹

5
6 ¹ Department of Forest Ecosystems and Society, Oregon State University, OR 97331,
7 USA

8 ² Department of Earth and Environmental Sciences, University of Illinois at Chicago,
9 Chicago, Illinois, USA

10 ³ Atmospheric, Earth and Energy Division, Lawrence Livermore National Laboratory,
11 7000 East Avenue, L-103, Livermore, CA 94550, USA

12 ⁴ Carnegie Institution for Science, 260 Panama St., Stanford, CA, USA, 94305

13 ⁵ USDA Forest Service, PNW Research Station, Corvallis, OR 97331, USA

14 ⁶ College of Earth, Ocean and Atmospheric Sciences, Oregon State University, OR
15 97331, USA

16 Corresponding author: Bharat Rastogi (bharat_rastogi@oregonstate.edu)

17
18 **Abstract**

19 Carbonyl sulfide (OCS) has recently emerged as a tracer for terrestrial carbon uptake.
20 While physiological studies relating OCS fluxes to leaf stomatal dynamics have been
21 established at leaf and branch scales and incorporated in global carbon cycle models, the
22 quantity of data from ecosystem-scale field studies remains limited. In this study, we
23 employ established theoretical relationships to infer ecosystem-scale plant OCS uptake
24 from mixing ratio measurements. OCS fluxes showed a pronounced diurnal cycle, with
25 maximum uptake during mid-day. OCS uptake was found to scale with independent
26 measurements of CO₂ fluxes over a 60-m-tall old-growth forest in the Pacific
27 Northwestern U.S. (45°49'13.76" N; 121°57'06.88") at daily and monthly timescales
28 under mid-high light conditions across the growing season in 2015. OCS fluxes were
29 strongly influenced by the fraction of downwelling diffuse light. Finally, we examine the
30 effect of sequential heatwaves on fluxes of OCS, CO₂ and H₂O. Our results bolster
31 previous evidence that ecosystem OCS uptake is strongly related to stomatal dynamics,
32 and measuring this gas improves constraints on estimating photosynthetic rates at the
33 ecosystem scale.

34

35 **1. Introduction**

36 Carbonyl Sulfide (OCS) is the most abundant sulfur gas in the atmosphere, with a mean
37 atmospheric concentration of ~500 ppt (parts per trillion), and therefore a significant part
38 of the tropospheric and stratospheric sulfur cycles, with implications for the global
39 radiation budget and ozone depletion (Johnson et al., 1993; Notholt et al., 2003). The
40 dominant sink of atmospheric OCS is vegetation (Kesselmeier and Merk, 1993; Kettle et
41 al., 2002; Montzka et al., 2007 and references therein), through rapid and irreversible
42 hydrolysis by the ubiquitous enzyme carbonic anhydrase (Protoschill-Krebs, Wilhelm, &

Deleted: tracked changes in soil moisture, and

44 Kesselmeier, 1996; Protoschill-Krebs and Kesselmeier, 1992). Recent advances in
45 spectroscopic technology have enabled continuous in-situ measurements of OCS on
46 timescales that are relevant to understanding stomatal function at the leaf-scale (Stimler
47 et al., 2010a, 2010b), branch scale (Berkelhammer et al., 2014) and the ecosystem scale
48 (Kooijmans et al., 2017; Wehr et al., 2017). An important distinction between OCS and
49 CO₂ cycling is the absence of a retroflux from actively photosynthesizing leaves (OCS
50 emissions have been reported from stressed crops following severe fungal infection;
51 Bloem et al., 2012). However, the normalized leaf uptake ratio of OCS:CO₂ (LRU;
52 Sandoval-Soto et al., 2005) is relatively constant at medium to high light levels (Maseyk
53 et al., 2014; Stimler et al., 2010), making it an excellent proxy for quantifying plant
54 productivity (GPP; Asaf et al., 2013; Billesbach et al., 2014; Blonquist et al., 2011). On
55 the other hand, both uptake and emissions of OCS from soils have been identified
56 (Whelan et al., 2016; Sun et al., 2015; Maseyk et al., 2014; Kesselmeier et al., 1999).

57 While ecosystem-scale measurements of OCS continue to establish links between OCS
58 uptake and GPP in different ecosystems (for a comprehensive list of ecosystem scale
59 studies readers are referred to Figure 2 in Whelan et al., 2018), inconsistencies persist.

60 For example, in an oak-savanna woodland in southern France Belviso et al. (2016) found
61 that OCS exchange was strongly influenced by photosynthesis during early morning
62 hours, while meaningful values of LRU could only be calculated for a few days in the
63 early afternoons. Commane et al. (2015) were unable to explain mid-summer emissions
64 of OCS at a mid-latitude deciduous forest. Uncertainties highlighted above argue for
65 field-scale measurements of OCS in a variety of ecosystems, particularly as OCS flux
66 predictions have recently been incorporated to inform estimates of plant productivity in
67 global carbon cycle models (Campbell et al., 2017a; Hilton et al., 2017; Launois et al.,
68 2015).

69
70 OCS fluxes have not been previously reported for old-growth forests, although a recent
71 study using flask samples inferred large uptake of OCS in coastal redwood forests in
72 northern California (Campbell et al., 2017b). Rastogi et al. (in revision) found large
73 drawdowns in mixing ratios of OCS at an old growth forest in the pacific northwestern
74 U.S., and significant uptake of this gas by various components of the ecosystem (leaves,
75 soils, and epiphytes). In this study, we report estimates of OCS fluxes from an old-growth
76 forest and place them in the context of ecosystem carbon and water cycling. Additionally,
77 we investigate the response of CO₂, H₂O and OCS fluxes to changes in the fraction of
78 downwelling diffuse radiation, as well as heat wave events through the growing season.
79 Technological constraints posed limitations in measuring fast-response OCS fluxes so
80 instead we combine continuous in-situ measurements of OCS mixing ratios above and
81 within the canopy with established theoretical equations for OCS uptake (see Berry et al.,
82 2013; Commane et al., 2015; Seibt et al., 2010) to characterize OCS fluxes using a simple
83 empirical model and compare them with ecosystem uptake of CO₂ from co-located eddy
84 covariance measurements.

85 86 **2. Methods**

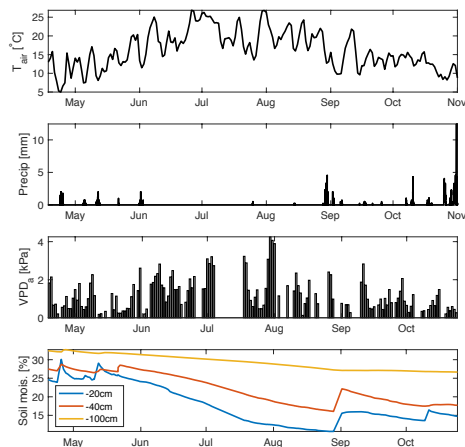
87 **2.1. Site Description**

88 Measurements were made at the Wind River Experimental Forest (WR), located within
89 the Gifford Pinchot National Forest in southwest Washington state, USA (45°49'13.76"

Deleted: While ecosystem-scale measurements of OCS continue to establish links between OCS uptake and GPP in different ecosystems (for a comprehensive list of ecosystem scale studies readers are referred to Figure 2 in Whelan et al., 2017), inconsistencies persist.

95 N; 121°57'06.88"; 371 m above sea level). The site is well studied and described in great
96 detail (Paw U et al., 2004; Shaw et al., 2004; Wharton and Falk, 2016; Winner et al.,
97 2004). The climate is classified as temperate oceanic with a strong summer drought. The
98 forest is 478 ha of preserved old-growth evergreen needle-leaf forest, with dominant tree
99 species of Douglas fir (*Pseudotsuga menziesii*) and Western hemlock (*Tsuga*
100 *heterophylla*). The tallest Douglas fir trees are between 50 and 60m, while the shade-
101 tolerant hemlocks are typically between 20-30 m high. Maximum rooting depth is 1–2 m
102 for the tallest, dominant Douglas-fir trees although most of the root biomass is
103 concentrated in the first 0.5 m (Shaw et al., 2014). The cumulative LAI is estimated to be
104 8-9 m² m⁻² (Parker et al., 2004). Additionally, the ecosystem hosts a large diversity of
105 mosses, lichens and other epiphytic plants, which play an important role in canopy OCS
106 dynamics (Rastogi et al., in revision). The soils are volcanic in origin, although most of
107 the forest surface is comprised of decaying organic matter (Shaw et al., 2004).

108
109 2.2. Study period: Measurements reported here are between April 18- Dec 31, 2015.
110 However, in early November an intake line at the top of the canopy was damaged after a
111 rainstorm. Measurements continued at the other intake heights (see sections 2.4 and 2.9).
112 Therefore, ecosystem fluxes and related analyses in this study cover 136 days between
113 April 18 and October 31, while chamber based soil fluxes are reported for the months of
114 August-December. Gaps in the time series due to analyzer maintenance correspond to Jun
115 26-28, July 6-17, August 4-7, August 24 and October 4-7. April-October roughly
116 corresponds to most of the growing season, although at this site GPP usually peaks early
117 in March-April, when soil moisture is high and ecosystem respiration flux is low, while
118 plant productivity is typically severely light and temperature limited in the months of
119 November-December (Wharton and Falk, 2016). Environmental conditions during the
120 measurement campaign are shown in Figure 1 are represent a typical Mediterranean-type
121 climate, with temperature peaking in July and minimal to no measured rainfall between
122 June and September. This results in high summertime atmospheric vapor pressure deficit
123 (VPDa), and soil moisture declines steadily through the summer period, with some
124 recharge following rare precipitation events in September and then more commonly in
125 October. The measurement period also encompasses three distinct heat waves,
126 characterized by anomalously high air temperatures and mid-day VPDa values (often
127 exceeding 4 kPa). We examine the response of OCS and CO₂ fluxes during these heat
128 waves.



129
130 Figure 1. Environmental conditions at Wind River during the measurement campaign.
131 daily mean air temperature (a), precipitation (b) mid-day VPDa (c) and soil moisture
132 measured at three depths (d) are shown.

133 2.3. CO₂ and H₂O eddy flux measurements: Carbon, water and energy fluxes have been
134 collected since 1998 at the Wind River AmeriFlux tower (US-wrc; Paw U et al. 2004).
135 For further details readers are referred to Falk et al., (2008; instrumentation and data
136 processing), and Wharton et al., (2012) and Wharton and Falk, (2016) for multi-year
137 carbon and water flux measurements and synthesis.

138
139 2.4. OCS measurements: A commercially available off-axis integrated cavity output
140 spectroscopy analyzer manufactured by Los Gatos Research Inc., (LGR; model 914-
141 0028) was deployed at the base of the tower in an insulated and temperature-controlled
142 shed. The instrument measures mixing ratios of OCS, CO₂, H₂O and CO simultaneously
143 at a maximal scan rate of 5Hz. The system uses a 4.87 μm cascade laser coupled to a high
144 finesse 800 cm³ optical cavity and light transmitted through the cavity is focused into a
145 cooled and amplified HgCdTe detector. OCS is detected at ~2050.40 cm⁻¹, CO₂ at
146 2050.56 cm⁻¹, CO at ~2050.86 cm⁻¹, and H₂O at ~2050.66 cm⁻¹. Pressure broadening
147 associated with changes in the concentration of water vapor in the samples is corrected
148 for in the analysis routine. Air was sampled through 0.25'' diameter PFA tubing using a
149 diaphragm pump at a flow rate of 2L min⁻¹, from inlets located at 70m (at the height of
150 the eddy flux instrumentation), 60m (canopy top), 20m, 10m, and 1m. The sampling
151 frequency was 0.1Hz and the sampling interval was 5 minutes. The first minute of each
152 sampling interval was removed to avoid any inter-sampling mixing. The remaining data
153 were checked for temperature and pressure fluctuations inside the measurement chamber,
154 and a moving window filter was used to eliminate any sudden outliers in the data. Mixing
155 ratios were aggregated to provide hourly means. For detailed information regarding
156 instrumentation and the measurement readers are referred to Rastogi et al (in revision),
157 Berkelhammer et al. (2014) and Belviso et al. (2016).

158 2.5. Calibration: Calibration was performed using ambient air stored in insulated tanks as
159 a secondary reference. Air was sampled into the analyzer daily, and tank pressure was
160 routinely monitored to check for leaks. Glass flasks were randomly sampled from
161 calibration tanks and measured against a NOAA GMD reference standard. Cross-
162 referencing revealed that the accuracy of the measurement was within the reported
163 minimum uncertainty of the instrument (of 12.6 pmol mol⁻¹; Berkelhammer et al., 2016).
164

165 2.6. Thermal Camera measurements: Leaf temperatures were measured from October 28,
166 2014 to January 28, 2016 using a FLIR A325sc thermal camera (FLIR System Inc.,
167 Wilsonville, OR), in which a FLIR IR 30-mm lens (focal length: 30.38 mm; field of
168 view: 15°×11.25°) was installed. The thermal camera has a pixel resolution of 320 × 240.
169 Within the field of view (FOV), spot sizes of a single pixel are 0.83 cm from 10-m
170 distance and 8.3 cm from 100-m distance. Manufacturer-reported errors in original
171 measured thermal temperatures are ±2 °C or ±2% of the measurements. The camera
172 model is identical to one used in another study at an AmeriFlux site in central Oregon
173 (US Me-2), and the detailed specifications can be found in Kim et al. (2016). To monitor
174 a larger canopy region, a pan-tilt unit (PTU) was used for motion control, allowing
175 multiple canopy thermal image acquisition within one motion cycle. We used a FLIR
176 PTU-D100E (FLIR System Inc., Wilsonville, OR; (<http://www.flir.com/mcs>) to move the
177 thermal camera vertically and horizontally at specific pan and tilt angles. We selected
178 five pan-tilt angle (PT) positions representing the upper canopy (i.e., ~40 to 60 m above
179 the forest floor) to estimate leaf temperatures in this study.

180 2.7. Diffuse light measurement and analyses: An SPN1 Sunshine Pyranometer (Delta-T
181 Devices Ltd., Cambridge, U.K.) was installed at the top of the canopy and collected direct
182 and diffuse shortwave downwelling radiation from April- December 2015. Measurements
183 were made every 1 min, and then aggregated to hourly means. We limited our analyses of
184 diffuse radiation data to include only mid-day hours (between 11am-1pm) to minimize
185 the influence of solar angles on diffuse radiation fractions. We defined three distinct
186 periods based on the ratio of diffuse radiation to total incoming solar radiation (*f_{diff}*).
187 Data were characterized as clear if *f_{diff}* < 0.2; partly cloudy if *f_{diff}* > 0.2 and *f_{diff}* < 0.8,
188 and overcast if *f_{diff}* > 0.8. ____

189 2.8. OCS flux estimation: ‘Canopy-scale leaf’ OCS flux was estimated using flux-
190 gradient similarity, following Commane et al., 2015.

$$F_{OCS} = F_{H_2O} \cdot \frac{\Delta_{OCS}}{\Delta_{H_2O}} + S_{OCS} \quad (1)$$

Deleted: $\frac{g_{OCS}}{g_{H_2O}}$

193 where F_{OCS} , F_{H_2O} , Δ_{OCS} and Δ_{H_2O} are the fluxes and gradients of OCS and H₂O
194 respectively and S_{OCS} is the change in storage flux of OCS. Change in storage flux is
195 subject to large uncertainties and estimates have been shown to vary depending on the
196 averaging time and vertical resolution of the storage profile (Yang et al., 2007),
197 horizontal resolution and site heterogeneity (de Araújo et al., 2010; Nicolini et al., 2018)
198 as well as canopy decoupling (Jocher et al., 2018). Since large parts of the canopy at the
199 site are decoupled from the bulk air at all times (Pyles et al., 2004), we inferred change in
200 storage as the height integrated change in the time derivative of mixing ratios between the
201 canopy top and above the canopy. Following Seibt et al., (2010) and Berry et al., (2013),

we assume that OCS is irreversibly and rapidly consumed inside leaves, such that the gradient between ambient air and the leaf interior effectively reduces to the ambient measured OCS mixing ratio: $\Delta_{OCS} \Delta_{H_2O}$.

where Δ_{OCS} is defined as the gradient of OCS between ambient air and the leaf intercellular spaces (χ is the mixing ratio of OCS and superscripts a and l refer to ambient and leaf respectively). In our study, χ_{OCS}^a is the measured mixing ratio at the canopy top (60m) instead of above canopy (70m) to account for turbulent transport between the canopy top and air that is above the canopy top. We use vapor pressure deficit (VPD) as the corresponding gradient for H_2O , under the key assumption that the intercellular leaf surfaces are saturated with water vapor. While VPD is usually calculated using air temperature, a more accurate calculation can be performed with leaf temperatures, which can deviate significantly from air temperatures (Kim et al. 2016), leading to significant differences between the VPD of ambient air and that at the leaf surface (Fig. 2a and 3d in this study). Previously leaf temperatures have been inferred from sensible heat fluxes, wind speed and air temperatures (e.g. Wehr et al., 2017), here we use explicit measurements of leaf skin temperatures to estimate leaf-air VPD (VPD_l). Analogous to Eq (3),

$$\Delta_{H_2O} = \chi_{H_2O}^l - \chi_{H_2O}^a = \frac{(e_l - e_a)}{P} = \frac{VPD_l}{P}, \quad (3)$$

where e_i is saturation vapor pressure in the leaf sub-stomatal cavity (kPa), using leaf skin temperature, e_a is the actual vapor pressure (kPa), P is the measured atmospheric pressure (kPa) at the tower top, and $\chi_{H_2O}^l$ and $\chi_{H_2O}^a$ (ppth) are the leaf and ambient H_2O mixing ratios at the canopy top. Finally, since gradients of OCS and H_2O are estimated between ambient air and the leaf intercellular spaces, these are normalized by the ratio of diffusivities of these two species in air (Seibt et al., 2010; Wohlfahrt et al., 2012).

F_{H_2O} was measured using eddy covariance at the tower top (70m). In high LAI forests with minimal exposed soil, such as those of the Pacific Northwest, fluxes of F_{H_2O} can be treated as a good proxy for transpiration, since soil evaporation is minimal. We excluded rainy days, as well as two days following rainfall, to only capture periods when F_{H_2O} can be assumed to be dominated by transpiration. Equation (1) was evaluated only under the condition $F_{H_2O} > 0.2 \text{ mmolm}^{-2}\text{s}^{-1}$. We restricted our analyses to daytime, when OCS flux is assumed to be related to leaf CO_2 uptake (Maseyk et al., 2014; Wehr et al., 2017).

Leaf Relative uptake was calculated following Seibt et al (2010).

$$LRU = \frac{F_{OCS}}{GPP} \cdot \frac{\chi_{CO_2}}{\chi_{OCS}}, \quad (5)$$

where GPP was estimated from CO_2 fluxes measured at the tower top, using a nighttime based partitioning approach (Reichstein et al., 2005), that was optimized for the site (Falk et al., 2008). Finally, canopy conductance (G_c) was estimated using a simple flux-gradient approach with the assumption that the canopy (or ecosystem) acts as a single big leaf.

Deleted: where F_{OCS} , F_{H_2O} ,
 Deleted: g_{OCS} and
 Deleted: g_{H_2O} are the fluxes and gradients of OCS and H_2O , respectively. Following Seibt et al., (2010) and Berry et al., (2013), we assume that OCS is irreversibly and rapidly consumed inside leaves, such that the gradient between ambient air and the leaf interior effectively reduces to the ambient measured OCS mixing ratio:
 Deleted: $g\Delta_{OCS}$
 Deleted: g_{OCS}

Deleted: g_{H_2O}

Deleted: F_{H_2O} was measured using eddy covariance at the tower top (70m). In high LAI forests with minimal exposed soil, such as those of the Pacific Northwest, fluxes of F_{H_2O} can be treated as a good proxy for transpiration, since soil evaporation should be minimal. We excluded rainy days, as well as two days following rainfall, to only capture periods when F_{H_2O} can be assumed to be dominated by transpiration. Equation (1) was evaluated only under the condition $F_{H_2O} > 0.2 \text{ mmolm}^{-2}\text{s}^{-1}$. We restricted our analyses to daytime, when OCS flux is assumed to be related to leaf CO_2 uptake (Maseyk et al., 2014; Wehr et al., 2017).

270
$$G_c = F_{H_2O} \cdot \frac{VPD_i}{P} \quad , \quad (6)$$

271
 272 2.9. Surface Fluxes: A long-term automatic soil survey chamber (Li-Cor 8100-104, 20
 273 cm diameter) was installed at three 0.03 m² surface sites in series, within 1 meter of each
 274 other. All plastic and rubber parts had been removed from the chamber and replaced with
 275 materials compatible with OCS measurements: stainless steel, PFA plastic, and Volara
 276 foam. Blank measurements were performed in the laboratory before deployment and
 277 OCS concentrations in the chamber were found to be statistically indistinguishable from
 278 incoming ambient concentrations. The stainless-steel chamber top opened and closed
 279 automatically on a timer. Gas was drawn through the chamber via a pump downstream of
 280 the analyzer, and the 3 Lmin⁻¹ flow rate was confirmed with a mass flow meter. When the
 281 chamber was open, ambient near-surface air was observed. When the chamber was
 282 closed, trace gas concentrations reached a stable state for at least 2 minutes during the 10-
 283 minute incubation time. The difference between the ambient concentration and the stable
 284 closed-chamber concentration were used to calculate the surface fluxes of OCS and CO₂.

285
$$F_{forest\ floor} = M_c \Delta\chi \cdot A^{-1} \quad , \quad (7)$$

286 where M_c is the measured flow rate into the chamber (converted from Lmin⁻¹ to mols⁻¹
 287 using the ideal gas law) and Δχ is the difference between mixing ratios of OCS or CO₂ in
 288 ambient air and the chamber and A is the surface area of the chamber. The minimum flux
 289 detectable with this method was 1.2 pmolm⁻²s⁻¹ uptake or production.

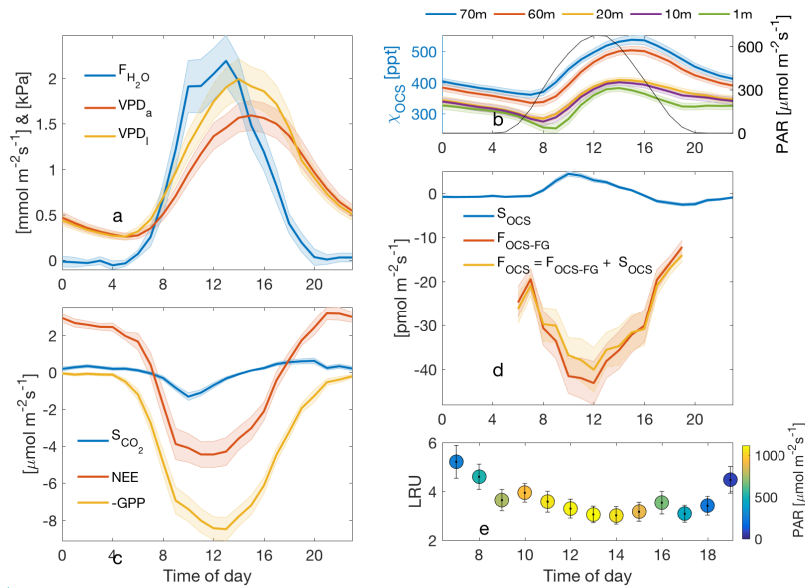
290 Care was taken to select sites characteristic of the surface, which was generally springy
 291 and covered in a mat of mosses and lichen. Surface flux observations were made at site 1
 292 from July 6 to 16, site 2 from August 13 to October 7, and site 3 from November 6 to
 293 December 2, 2015. The first site was visually similar to the subsequent two sites at the
 294 surface, though the chamber base of the first site was installed into the moss layer and a
 295 barely decomposed fallen tree. When a soil sample was attempted to be extracted from
 296 the footprint of the chamber base, several liters of intact wood litter were removed. The
 297 influence of the developed soil on site 1 is therefore considered minimal. Site 2 was
 298 selected nearby and observations were made until a dominant tree fell on the soil
 299 chamber. The chamber was repaired and re-installed a month later at site 3 and
 300 observations continued without incident until the chamber was removed in advance of the
 301 soil freezing.

302 **3. Results and Discussion:**

303 3.1. Ecosystem fluxes: The composite diurnal cycles for CO₂, water vapor and OCS and
 304 fluxes are shown (Fig. 2a-d). The total ecosystem flux of OCS (F_{OCS}; Fig 2.d) follows a
 305 pronounced diurnal cycle that peaks during mid-day. The vertical profile of mixing ratios
 306 measured throughout the canopy is also shown (Fig.2.b). OCS mixing ratios are highest
 307 at the canopy top and lowest near the forest floor, but mixing ratios increase from the
 308 early morning to mid-afternoon. Together these processes are indicative of ecosystem
 309 uptake and downward entrainment of boundary layer air (Rastogi et al., *in press*). The
 310 shape of the F_{OCS} curve is very similar to those of net and gross carbon fluxes (Fig 2.b-c),
 311 although F_{OCS} was consistently negative during daylight hours. Leaf relative uptake, a
 312 ratio of F_{OCS}:GPP normalized by the mean mixing ratios of OCS:CO₂, showed a strong

Deleted: c
Deleted: b
Deleted: daylight hours
Deleted: right y-axis and orange lines in
Deleted: . While entrainment helps explain the diurnal cycle of observed mixing ratios, this flux integrates to zero at daily and longer time scales
Formatted: Font:Italic
Deleted: revision).
Deleted: throughout the 24-hour period, implying ecosystem uptake during nighttime and daylight hours. While nighttime uptake of OCS (mean nighttime flux ~ -10 ± 1 pmolm ⁻² s ⁻¹) is likely due to a combination of soil, epiphyte, and vascular plant uptake due from partially closed stomata, daytime uptake is likely dominated by vascular plant stomatal activity.

§28 light dependence (Fig. 2e). High-light, mid-day values ranged between 3-4, which is
 §29 higher than those observed at other forest systems (Kooijmans et al., 2017; Wehr et al.,
 §30 2017) but well within the spread of values obtained in a recent meta-analysis of OCS
 §31 studies for vegetated ecosystems (Whelan et al., 2018). The diurnal cycle was found to be
 §32 asymmetric, with peak values observed in the early morning, when stomatal conductance
 §33 is likely to be high (Winner et al., 2004), but GPP is limited by low light. It is important
 §34 to note that LRU is likely influenced by large amounts of epiphyte and understory
 §35 vegetation, which assimilate OCS even at times when ecosystem CO₂ uptake is low or
 §36 zero. Epiphytic assimilation of OCS is highly influenced by moisture content (Gimeno et
 §37 al., 2017) and is typically higher through the night and in the early mornings at this site
 §38 (Rastogi et al., in press). Moreover, in tall old-growth forests, leaf area is vertically
 §39 distributed over a much larger part of the canopy compared to other forests (Parker et al.,
 §40 2004). While leaves at the canopy top exercise tight stomatal control to limit water loss
 §41 and minimize hydraulic failure (Woodruff et al., 2007) leaves lower down in the canopy,
 §42 including those of understory vegetation, likely impose less stomatal control of
 §43 transpiration (Winner et al., 2004). Lower-canopy leaves may therefore continue to
 §44 disproportionately assimilate OCS, even under low rates of carbon assimilation (as CO₂
 §45 uptake is additionally light limited).



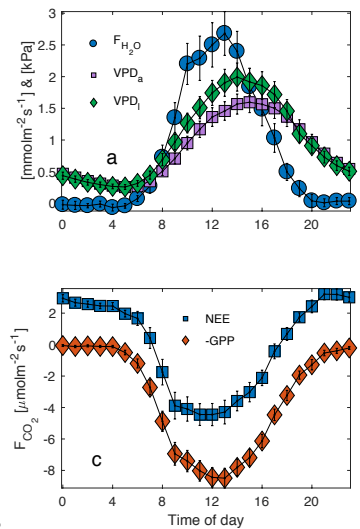
§46
 §47 **Figure 2. Diurnal cycle of measured H₂O flux (blue curve) and VPD estimated from air and leaf**
 §48 **temperatures (red and yellow curves, respectively; a), diurnal cycles of OCS mixing ratio profiles**
 §49 **measured along the canopy (left axis) and mean PAR (right axis; b), inferred storage flux of**
 §50 **CO₂ (blue curve), measured turbulent flux of CO₂ (NEE; red curve) and estimated flux of**
 §51 **GPP (yellow curve, plotted as a negative quantity to show uptake; are shown in c), diurnal**

Deleted: .

Deleted: levels

Deleted: revision

Formatted: Font:(Default) Times New Roman



Deleted:

Deleted: 2

Deleted: circles

Formatted: Font:(Default) Times New Roman

Field Code Changed

Deleted: purple squares

Deleted: green diamonds

Deleted: estimated

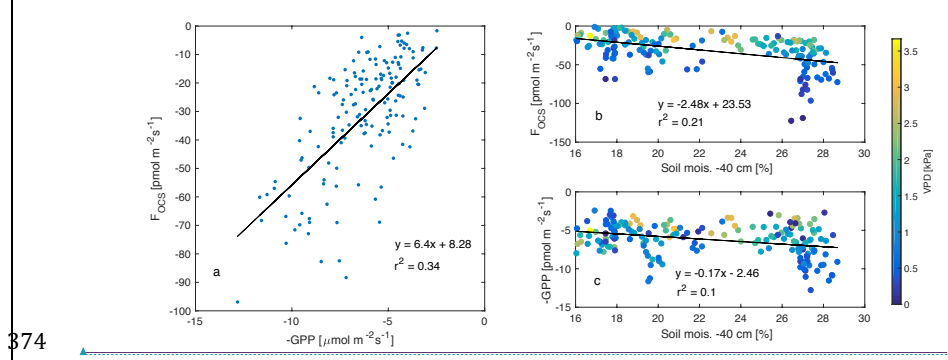
Deleted: flux (circles,

Deleted: mixing ratio profile

Deleted: blue squares and red diamonds;

364 cycle of change in storage flux of OCS (S_{OCS} ; blue curve; d), estimated flux of OCS using
 365 flux-gradient similarity (F_{OCS-FG} ; red curve in d) and the sum of the two fluxes (F_{OCS} ;
 366 yellow curve in d), and mean diurnal cycle of leaf relative uptake estimated according to eq.
 367 (5), shown in (e), and colored according to mean PAR. Shaded regions (in a-d) and
 368 vertical bars (in e) represent one standard error.

369 3.2. Daily and seasonal dynamics: Daytime fluxes of OCS (estimated as fluxes when
 370 PAR was higher than $100 \mu\text{mol m}^{-2}\text{s}^{-1}$) were correlated to independent estimates of GPP
 371 (Fig. 3a), and uptake of both OCS and CO_2 reduced as soil moisture declined. Variability
 372 in the relationship between fluxes of OCS and CO_2 and soil moisture was related to VPD,
 373 which fluctuated as a response of changing cloud cover (discussed later in sec. 3.4).



374 Figure 3. F_{OCS} was linearly correlated to GPP (plotted as a negative quantity to show
 375 ecosystem uptake; a), while both F_{OCS} and GPP reduced as a function of decreasing soil
 376 moisture (b-c). Data presented here are mid-day means, data in (b-c) are colored
 377 according to VPD.
 378

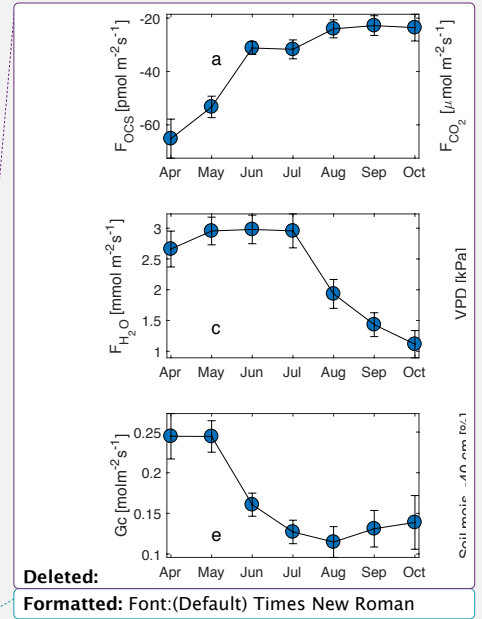
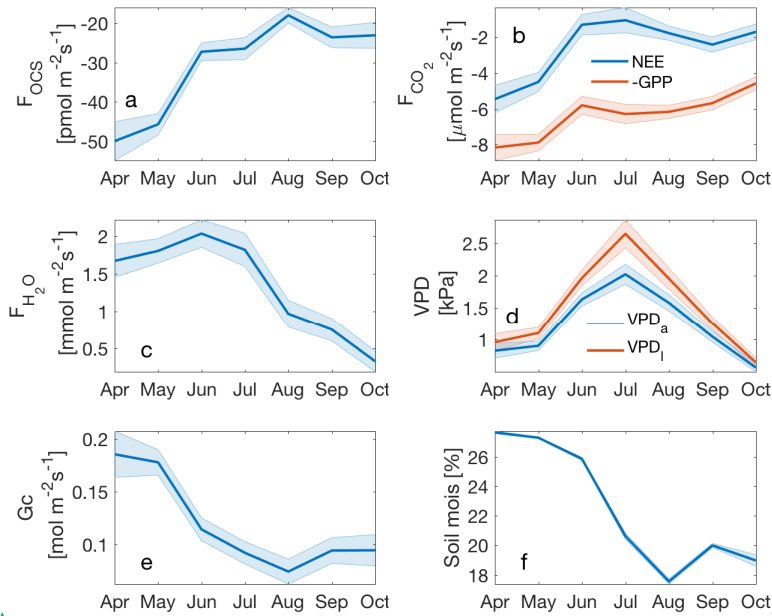
379 Ecosystem uptake of OCS and CO_2 (as well as GPP) was highest in April (Fig. 4a), and
 380 declined as the soil drought progressed (Fig. 4f). Mean monthly maximum OCS flux was
 381 estimated as $-61 \pm 6 \text{ pmol m}^{-2}\text{s}^{-1}$, while daily mean maximum GPP over this period was
 382 estimated as $10 \pm 1 \mu\text{mol m}^{-2}\text{s}^{-1}$ (plotted as a negative quantity in Fig. 4b to show
 383 ecosystem uptake). While the steepest declines in F_{OCS} , NEE and GPP happened between
 384 the months of May and June, F_{OCS} continued to decline through the rest of the summer,
 385 with a minimum in August, and remaining low in September and October. CO_2 fluxes
 386 flattened between June-September, before declining again in October. While uptake of
 387 OCS and CO_2 followed similar patterns, H_2O flux remained high until mid-summer (Fig.
 388 4c) and decreased in August, presumably due to a combination of high VPD (Fig. 4d) and
 389 declining soil moisture (Fig. 4f), as plants exercised greater control over stomata. This
 390 can be clearly seen in the seasonal cycle of canopy conductance (G_c ; Fig. 4e). Mean
 391 monthly G_c was highest in the months of April and May, and then declined in response to
 392 increasing VPD and decreasing soil moisture, before increasing again slightly in
 393 September and October following soil recharge and decreased VPD due to precipitation
 394 events. In October, soil water recharge, several rain-free days (Fig. 1), and lower VPD

Deleted: (calculated only during daylight hours, colors
 Deleted: Photosynthetically active radiation; d). Vertical
 bars indicate
 Deleted: .

Formatted: Font:(Default) Times New Roman

Formatted: Font:Subscript
 Deleted: before plunging

400 (Fig. 4d) do not result in increased gas exchange, likely due to downregulation of
 401 photosynthesis (Eastman and Camm, 1995), induced by photoprotective changes in the
 402 xanthophyll cycle (Adams and Demmig-Adams, 1994).



Deleted:
 Formatted: Font:(Default) Times New Roman

403
 404 Figure 4. Monthly means for daytime F_{OCS} (a), NEE and -GPP (blue and red curves; b),
 405 water vapor flux (c), VPD_a and VPD_l (blue and red curves respectively; d), canopy
 406 conductance (G_c ; e), and soil moisture at -40cm depth (f). Vertical bars indicate standard
 407 error.

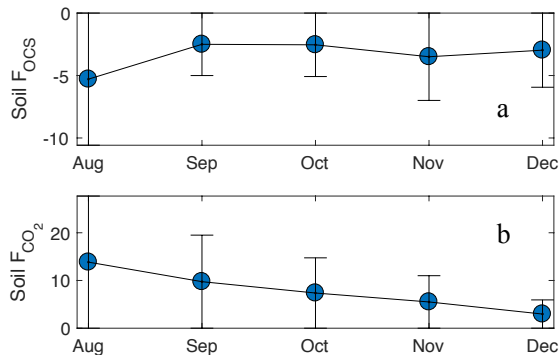
Deleted: ,
 Deleted: red circles and
 Deleted: squares
 Deleted: squares
 Deleted: circles

408 3.3. Surface Fluxes: Forest floor OCS fluxes were observed from 3 sites in series and
 409 within 1 m of each other. Site 1 had approximately twice the OCS uptake compared to
 410 the subsequent two sites and had a substantial layer of intact woody debris under the
 411 chamber footprint. Site 2 and 3 had OCS fluxes similar to previous surface fluxes
 412 reported for forests (Whelan et al., 2018). For all sites, there was no clear diurnal
 413 pattern. For site 2, uptake immediately following chamber installation was higher (~6
 414 $\text{pmol m}^{-2}\text{s}^{-1}$) than fluxes later on (all $<6 \text{ pmol m}^{-2}\text{s}^{-1}$) when temperatures were lower (Fig
 415 5). Site 3 did not have high uptake after chamber installation, and had consistent fluxes
 416 between the detection limit and $-6.2 \text{ pmol m}^{-2}\text{s}^{-1}$ for the first few weeks. When ambient
 417 air temperatures dropped below freezing, uptake remained unchanged, except for the
 418 largest uptake observed (6 to $12 \text{ pmol m}^{-2}\text{s}^{-1}$) during two events when average air
 419 temperature fluctuated from a cooling to warming trend. Soil temperature never dropped
 420 below freezing during the experiment and was generally colder over time. We did not
 421 observe any OCS emissions from the chamber based measurements, consistent with

428 recent studies that find that cooler, moist (Maseyk et al., 2014; Sun et al., 2016; Whelan
429 et al., 2016) and radiation limited (Kitz et al., 2017) soils do not emit OCS.

430 Surface CO₂ emissions exhibited a relationship with temperature, where highest
431 production (~25 μmol m⁻²s⁻¹) corresponded with temperatures ~15°C, and maximum flux
432 values decreased for warmer and colder temperatures. CO₂ emissions had a diurnal
433 pattern, with lowest emissions at night and maximum emissions in late morning to mid-
434 afternoon. No obvious relationship emerges from CO₂ emission and OCS uptake, though
435 the high OCS uptake events in late November and early December have a linear
436 relationship with CO₂ emissions. For sites 2 and 3, the ratio of OCS emission to CO₂
437 production, normalized by the concentration of OCS and CO₂ in the closed chamber, was
438 between -0.25 and -3.5 with a mean of -1. In contrast, the same ratio for site 1 varied
439 from -5 to -19 with a mean of -10.

440



441

442 Figure 5. Surface F_{OCS} and F_{CO₂} from chamber measurements (brown squares in a-b)
443 from sites 2 and 3. Site 1 was atypical (see section 2.7) and therefore fluxes are not
444 shown. Values for site 1 F_{OCS} and F_{CO₂} were -22 ± 0.3 pmolm⁻²s⁻¹ and -83 ± 2 μmolm⁻²s⁻¹
445 respectively. Error bars indicate standard deviation.

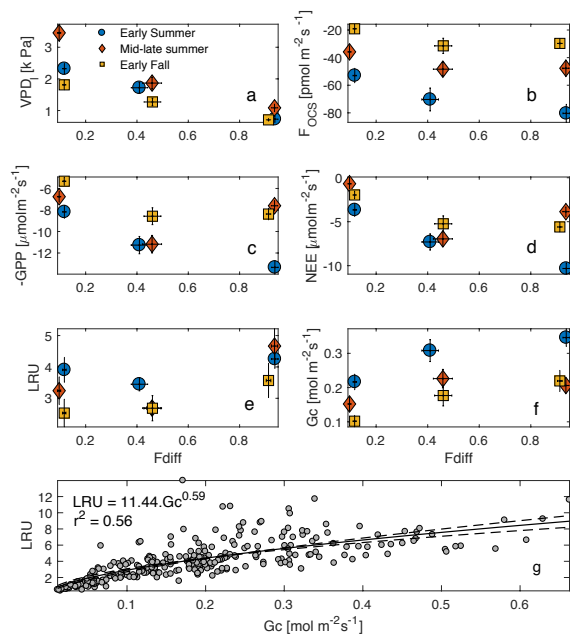
446 3.4. Sensitivity to diffuse light: Mid-day fluxes of OCS and CO₂ were found to be
447 sensitive to changes in the fraction of ~~diffuse~~ total incoming shortwave radiation (*fdiff*;
448 Figure 6b-c). For these analyses, data were separated into three periods corresponding to
449 early summer (DOY 109-180), mid-late summer (DOY 180-240) and early fall (DOY
450 240-297), and binned into three categories: clear sky conditions, partly cloudy, and
451 overcast, defined in sec. 2.7. Mid-day VPD was highest under clear sky conditions and
452 lowest under overcast skies, but was most different across the three periods, during clear
453 skies (Fig. 6a). Consequently, OCS and CO₂ uptake was highest (most negative fluxes)
454 under overcast conditions during the early summer, and generally declined as *fdiff*
455 decreased across all time periods (Fig. 6b-d). Across the three periods, the rate of
456 decrease was much higher as *fdiff* changed from partially cloudy to clear. During the mid-
457 late summer, however, (red diamonds in Fig. 6a-f), the diffuse light effect resulted in
458 GPP and NEE being almost as high as during the early summer. F_{OCS} was also highest
459 under partially cloudy skies during this time, and only showed a very weak decline under

Deleted: diffused:

461 completely overcast conditions. Overall, the behavior of OCS and CO₂ fluxes was similar
462 during the later time periods. Leaf relative uptake (LRU; calculated according to eq. 5)
463 was lowest under partly clear skies and highest under overcast conditions. This is because
464 under highly diffuse conditions, carbon uptake is additionally limited by light, whereas
465 F_{OCS} is not (Wehr et al., 2017; Maseyk et al., 2014). The shape of the LRU curves can
466 additionally be explained by examining canopy conductance (G_c; Fig. 6f), which was
467 also higher under overcast skies. LRU increased with G_c across all three periods (Fig.
468 6g), and appeared to be constant for G_c greater than ~400 mmolm⁻²s⁻¹.

469 The diffuse light enhancement of stomatal and canopy conductance is well documented
470 across a range of forest ecosystems (Alton et al., 2007; Cheng et al., 2015; Hollinger et
471 al., 2017; Urban et al., 2007; Wharton et al., 2012). Lower VPD (Fig. 6a) and light levels
472 allow plants to keep stomata open at mid-day and continue fixing CO₂. Lower VPD
473 reduces transpirational losses, and the lack of VPD-induced partial stomatal closure
474 reduces the resistance to CO₂ diffusion into the leaf. Correspondingly, the less directional
475 nature of diffuse solar radiation allows greater penetration into the canopy, thus
476 increasing photosynthesis across the entire canopy, even as a reduction in canopy top leaf
477 photosynthesis is observed due to a reduction in total radiation. In a multi-year analysis at
478 Wind River, Wharton et al., (2012) found that cloudy and partly cloudy sky conditions
479 during the peak-growing season lead to an increase in CO₂ uptake. During our study, G_c
480 was generally higher in the early growing season, but increased as sky conditions
481 changed from clear skies to overcast. This increase was similar across the three time
482 periods, even as the response of OCS and CO₂ fluxes was different across these periods.
483 This indicates that declining soil moisture (Fig. 3b-c) potentially limits gas exchange as
484 the summer progresses, even as canopy conductance can be reasonably high under
485 overcast skies. It is important to note that in the absence of concurrent leaf and root water
486 potential measurements, it is not possible to attribute reduction in gas exchange due to
487 declining soil moisture.

Deleted: likely



489

490 Figure 6. Mid-day VPD_i, F_{OCS}, NEE and GPP plotted against the fraction of diffuse
 491 downwelling shortwave radiation (a-d) for early summer, mid-late summer and early fall
 492 of 2015 (these periods are defined in Section 3.4). High values on the x-axis indicate
 493 completely overcast or cloudy conditions, whereas as low values indicated clear skies.
 494 LRU increases with increasing *f_{diff}* during each period but the increase is most
 495 pronounced in the early summer (e). Gc increases from clear to partly cloudy conditions
 496 across the three periods and plateaus during overcast sky conditions (f). Vertical bars
 497 indicate 1 standard error. Across the three periods, LRU increased with Gc, and levelled
 498 off at Gc values greater than ~ 0.5 mol m⁻²s⁻¹ (g).

499 3.5. Response to heat waves: 2015 was the warmest year in large parts of the Pacific
 500 Northwest since records began in the 1930s (Dalton et al., 2017). We observed three
 501 distinct heat waves during the 2015 summer. These were in early June (DOY 157-160),
 502 end of June- early July (DOY 175-188) and late July-early August (DOY 210-213). The
 503 three heat waves are shown as red, yellow and dark purple bars in Fig. 7; the overall time
 504 series is shown in blue (daytime means are plotted for all variables, where daytime is
 505 defined as PAR exceeding 100 μmol m⁻²s⁻¹). Additionally, boxplots for ‘non-heatwave’
 506 and ‘heatwave’ days are shown (labelled as No HW and HW respectively). Mid-day
 507 temperatures exceeded 30°C during these heat wave events, while VPD-leaf exceeded 3
 508 kPa during the first heat wave and increased to a mean daily maximum of 5.1 kPa during
 509 the last event (Fig. 7b). The canopy was a net source of CO₂ during all three events, while
 510 mid-day means for NEE were usually negative (implying CO₂ sink) before and after the
 511 heat wave periods (Fig. 7c). During the first event, F_{OCS} was similar to days immediately

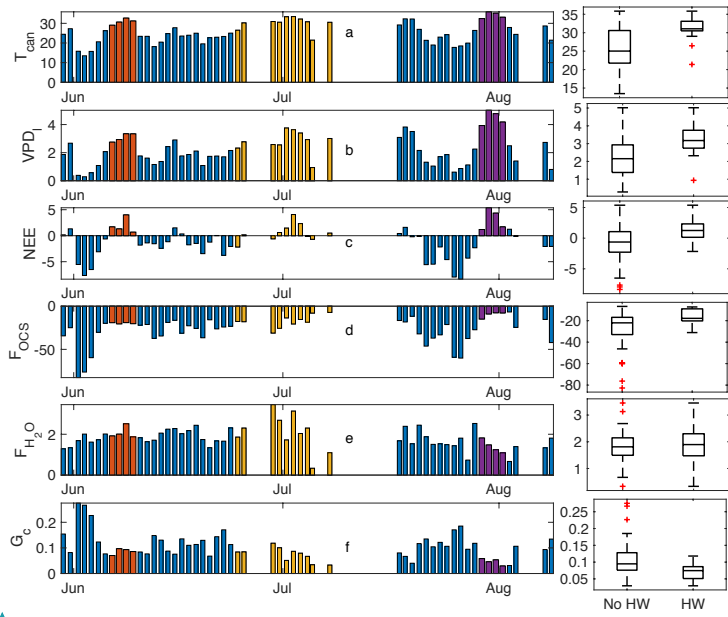
Deleted: lines
 Deleted: mid-day
 Deleted:).
 Deleted: 3
 Deleted: 7b

\$17 prior (Fig. 7d). The third event lead to a reduction in F_{OCS} , even though the canopy had
 \$18 received some rainfall in the preceding weeks (Fig. 1c). Overall, mean daytime OCS
 \$19 uptake decreased from -27 [$\mu\text{mol m}^{-2}\text{s}^{-1}$] in 'non-heatwave' days (daytime means
 \$20 presented as blue bars in Fig. 7) to -16 [$\mu\text{mol m}^{-2}\text{s}^{-1}$] during 'heatwave' days (daytime
 \$21 means from data presented as red, yellow and purple bars in Fig. 7). Water vapor fluxes
 \$22 (Fig. 7e) increased during the first heat wave, compared to days immediately prior. The
 \$23 increased water vapor flux is likely form an increase in transpiration under high VPD_l
 \$24 (red bars in Fig. 7b), that ensures a steady transpirational flux (purple bars in Fig. 7e).
 \$25 F_{H_2O} was not significantly different between 'heatwave' and 'non-heatwave' days
 \$26 (boxplots in Fig. 7e) even as VPD_l was significantly higher during these events leading to
 \$27 a suppression in canopy conductance (Fig. 7f).

Deleted: 7c), but the canopy became a net source of CO_2 during all three events (Fig.
 Deleted: events

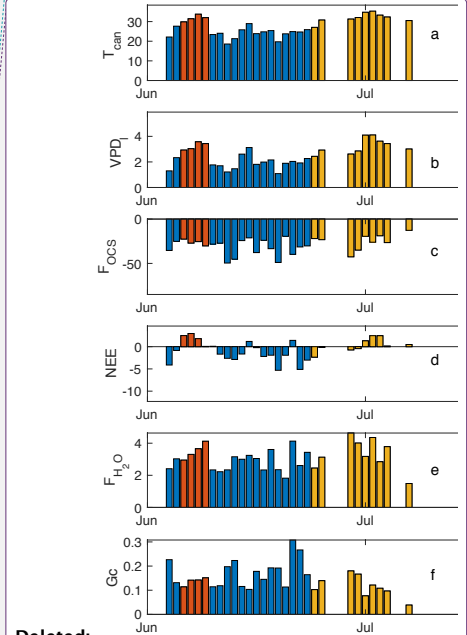
Deleted:). Even as canopy conductance (Fig. 7f) is reduced under the third heatwave, high VPD_l

Deleted: 7e).



\$28
 \$29 Figure 7. Daytime means (defined as periods when $PAR > 100 \mu\text{mol m}^{-2}\text{s}^{-1}$) for three heat
 \$30 wave periods (plotted as red, yellow and purple, while the overall time series is shown in
 \$31 blue). Variables displayed are canopy temperature ($^{\circ}\text{C}$; a), VPD_l -leaf (b), F_{OCS} (c), NEE
 \$32 (d), water vapor flux (e), and canopy conductance (G_c , f). Units for each panel are the
 \$33 same as specified in previous figures.

Formatted: Font:(Default) Times New Roman



Deleted:
 Deleted: Mid-day
 Deleted: 11am-1pm local time

\$34 **4. Conclusions**

\$35 Over hourly, daily and seasonal timescales, estimates of F_{OCS} generally tracked
 \$36 fluctuations in GPP, implying stomatal control of carbon, water, and OCS fluxes at the
 \$37 site. We used continuous in-situ measurements of OCS mixing ratios, collocated
 \$38 measurements of water vapor fluxes, and air and canopy temperatures to calculate OCS

Formatted: Line spacing: at least 12 pt

548 uptake. We found the forest to be a large sink for OCS, with sink strength peaking during
549 daylight hours. The mean LRU was ~ 4, and varied in response to changing light
550 conditions and canopy conductance. These LRUs are larger than observed from other
551 ecosystem scale studies, but well within the range of reported values (Whelan et al.,
552 2018; Sandoval-Soto et al., 2005). The forest surface was found to be a soil moisture
553 dependent sink of OCS. Ecosystem fluxes of OCS and CO₂ were found to be strongly
554 sensitive to the ratio of diffuse:direct radiation reaching the top of the canopy. Uptake of
555 both OCS and CO₂ increased as sky conditions changed from clear to partly cloudy. A
556 much smaller increase in uptake was observed as sky conditions changed from partly
557 cloudy to overcast, except during the early summer, when soil moisture was not limiting.
558 This change was mediated by the sensitivity of stomata to changing cloudiness and soil
559 moisture, as estimated from canopy conductance. Finally, we examined the response of
560 OCS, CO₂ and H₂O fluxes on heatwaves, and found that sequential heatwaves lead to
561 suppression in stomatal gas exchange of OCS and CO₂ fluxes, but not in the flux of water
562 vapour.

Deleted:

Deleted: all three

563 Our results support the growing body of work that suggests ecosystem-scale OCS uptake
564 is controlled by stomatal dynamics. While moist old-growth forests in Pacific
565 Northwestern U.S. do not represent a very large fraction of the global terrestrial surface
566 area, results from this study are likely relevant for other old-growth forests, particularly
567 high LAI and very wet forests with extensive epiphyte cover, which are widespread in the
568 humid tropics.

569 Acknowledgements:

570 This work was partly funded by NASA SBIR Phase II award NNX12CD21P to LGR,
571 Inc. (“Ultrasensitive Analyzer for Realtime, In-Situ Airborne and Terrestrial
572 Measurements of OCS, CO₂, and CO.”). We would like to thank the US Forest Service
573 and the University of Washington for letting us use the research facility at Wind River. In
574 particular, we wish to sincerely acknowledge Ken Bible and Matt Schroeder for their help
575 with setting up the experiment as well as maintenance throughout the measurement
576 campaign. Data collected and used in this study can be accessed at
577 ftp.fsl.orst.edu/rastogib/Biogeosciences2018_Rastogi.

578 References:

579 Adams, W. W. and Demmig-Adams, B.: Carotenoid composition and down regulation of
580 photosystem II in three conifer species during the winter, *Physiol. Plant.*, 92(3), 451–458,
581 doi:10.1111/j.1399-3054.1994.tb08835.x, 1994.

582 Alton, P. B., North, P. R. and Los, S. O.: The impact of diffuse sunlight on canopy light-
583 use efficiency, gross photosynthetic product and net ecosystem exchange in three forest
584 biomes, *Glob. Chang. Biol.*, 13(4), 776–787, doi:10.1111/j.1365-2486.2007.01316.x,
585 2007.

586 Asaf, D., Rotenberg, E., Tatarinov, F., Dicken, U., Montzka, S. A. and Yakir, D.:
587 Ecosystem photosynthesis inferred from measurements of carbonyl sulphide flux, *Nat.*

- 590 *Geosci.*, 6(3), 186–190, doi:10.1038/ngeo1730, 2013.
- 591 Belviso, S., Reiter, I. M., Loubet, B., Gros, V., Lathièrè, J., Montagne, D., Delmotte, M.,
592 Ramonet, M., Kalogridis, C., Lebegue, B., Bonnaire, N., Kazan, V., Gauquelin, T.,
593 Fernandez, C. and Genty, B.: A top-down approach of surface carbonyl sulfide exchange
594 by a Mediterranean oak forest ecosystem in Southern France, *Atmos. Chem. Phys.*
595 *Discuss.*, (June 2012), 1–25, doi:10.5194/acp-2016-525, 2016.
- 596 Berkelhammer, M., Asaf, D., Still, C., Montzka, S., Noone, D., Gupta, M., Provencal, R.,
597 Chen, H. and Yakir, D.: Constraining surface carbon fluxes using in situ measurements of
598 carbonyl sulfide and carbon dioxide, *Global Biogeochem. Cycles*, 28(2), 161–179,
599 doi:10.1002/2013GB004644, 2014.
- 600 Berkelhammer, M., Steen-Larsen, H. C., Cosgrove, A., Peters, A. J., Johnson, R.,
601 Hayden, M. and Montzka, S. A.: Radiation and atmospheric circulation controls on
602 carbonyl sulfide concentrations in the marine boundary layer, *J. Geophys. Res.*, 121(21),
603 13,113–13,128, doi:10.1002/2016JD025437, 2016.
- 604 Berry, J., Wolf, A., Campbell, J. E., Baker, I., Blake, N., Blake, D., Denning, A. S.,
605 Kawa, S. R., Montzka, S. A., Seibt, U., Stimler, K., Yakir, D. and Zhu, Z.: A coupled
606 model of the global cycles of carbonyl sulfide and CO₂: A possible new window on the
607 carbon cycle, *J. Geophys. Res. Biogeosciences*, 118(2), 842–852,
608 doi:10.1002/jgrg.20068, 2013.
- 609 Billesbach, D. P., Berry, J. A., Seibt, U., Maseyk, K., Torn, M. S., Fischer, M. L., Abu-
610 Naser, M. and Campbell, J. E.: Growing season eddy covariance measurements of
611 carbonyl sulfide and CO₂ fluxes: COS and CO₂ relationships in Southern Great Plains
612 winter wheat, *Agric. For. Meteorol.*, 184, 48–55, doi:10.1016/j.agrformet.2013.06.007,
613 2014.
- 614 Bloem, E., Haneklaus, S., Kesselmeier, J. and Schnug, E.: Sulfur fertilization and fungal
615 infections affect the exchange of H₂S and COS from agricultural crops, *J. Agric. Food*
616 *Chem.*, 60(31), 7588–7596, doi:10.1021/jf301912h, 2012.
- 617 Blonquist, J. M., Montzka, S. A., Munger, J. W., Yakir, D., Desai, A. R., Dragoni, D.,
618 Griffis, T. J., Monson, R. K., Scott, R. L. and Bowling, D. R.: The potential of carbonyl
619 sulfide as a proxy for gross primary production at flux tower sites, *J. Geophys. Res.*
620 *Biogeosciences*, 116(4), 1–18, doi:10.1029/2011JG001723, 2011.
- 621 Campbell, J. E., Berry, J., Seibt, U., Smith, S., Nature, S. M.- and 2017, U.: Large
622 historical growth in global terrestrial gross primary production, *nature.com*, 544(7468),
623 84 [online] Available from: <https://www.nature.com/articles/nature22030> (Accessed 29
624 January 2018a), 2017.
- 625 Campbell, J. E., Whelan, M. E., Berry, J. A., Hilton, T. W., Zumkehr, A., Stinecipher, J.,
626 Lu, Y., Kornfeld, A., Seibt, U., Dawson, T. E., Montzka, S. A., Baker, I. T., Kulkarni, S.,
627 Wang, Y., Herndon, S. C., Zahniser, M. S., Commane, R. and Loik, M. E.: Plant Uptake
628 of Atmospheric Carbonyl Sulfide in Coast Redwood Forests, *J. Geophys. Res.*

- 629 Biogeosciences, 122(12), 3391–3404, doi:10.1002/2016JG003703, 2017b.
- 630 Cheng, S. J., Bohrer, G., Steiner, A. L., Hollinger, D. Y., Suyker, A., Phillips, R. P. and
631 Nadelhoffer, K. J.: Variations in the influence of diffuse light on gross primary
632 productivity in temperate ecosystems, *Agric. For. Meteorol.*, 201, 98–110,
633 doi:10.1016/j.agrformet.2014.11.002, 2015.
- 634 Commane, R., Meredith, L. K., Baker, I. T., Berry, J. A., Munger, J. W., Montzka, S. A.,
635 Templer, P. H., Juice, S. M., Zahniser, M. S. and Wofsy, S. C.: Seasonal fluxes of
636 carbonyl sulfide in a midlatitude forest, *Proc. Natl. Acad. Sci.*, 112(46), 14162–14167,
637 doi:10.1073/pnas.1504131112, 2015.
- 638 Dalton, M. M., Dello, K. D., Hawkins, L., Mote, P. W. and Rupp, D. E.: The third
639 Oregon climate assessment report, Oregon Clim. Chang. Res. Institute, Coll. Earth,
640 Ocean Atmos. Sci. Oregon State Univ. Corvallis, OR, 2017.
- 641 Eastman, P. A. K. and Camm, E. L.: Regulation of photosynthesis in interior spruce
642 during water stress: changes in gas exchange and chlorophyll fluorescence, *Tree Physiol.*,
643 15(4), 229–235 [online] Available from: <http://dx.doi.org/10.1093/treephys/15.4.229>,
644 1995.
- 645 Falk, M., Wharton, S., Schroeder, M., Ustin, S. L. and Paw U, K. T.: Flux partitioning in
646 an old-growth forest: seasonal and interannual dynamics, *Tree Physiol.*, 28(4), 509–520,
647 doi:10.1093/treephys/28.4.509, 2008.
- 648 Gimeno, T. E., Ogée, J., Royles, J., Gibon, Y., West, J. B., Burrell, R., Jones, S. P.,
649 Sauze, J., Wohl, S., Benard, C., Genty, B. and Wingate, L.: Bryophyte gas-exchange
650 dynamics along varying hydration status reveal a significant carbonyl sulphide (COS)
651 sink in the dark and COS source in the light, *New Phytol.*, 215(3), 965–976,
652 doi:10.1111/nph.14584, 2017.
- 653 Hilton, T., Whelan, M., Zumkehr, A., ... S. K.-N. C. and 2017, U.: Peak growing season
654 gross uptake of carbon in North America is largest in the Midwest USA, *nature.com*,
655 7(6), 450 [online] Available from: <https://www.nature.com/articles/nclimate3272>
656 (Accessed 29 January 2018), 2017.
- 657 Hollinger, A. D. Y., Kelliher, F. M., Byers, J. N., Hunt, J. E., McSeveny, T. M., Weir, L.,
658 Ecology, S. and Jan, N.: Carbon Dioxide Exchange between an Undisturbed Old-Growth
659 Temperate Forest and the Atmosphere Published by : Wiley Stable URL :
660 <http://www.jstor.org/stable/1939390> REFERENCES Linked references are available on
661 JSTOR for this article : You may need to log , , 75(1), 134–150, 2017.
- 662 Johnson, J. E., Bandy, A. R., Thornton, D. C. and Bates, T. S.: Measurements of
663 atmospheric carbonyl sulfide during the NASA Chemical Instrumentation Test and
664 Evaluation project: Implications for the global COS budget, *J. Geophys. Res.*, 98(D12),
665 23443, doi:10.1029/92JD01911, 1993.
- 666 Kim, Y., Still, C. J., Hanson, C. V., Kwon, H., Greer, B. T. and Law, B. E.: Canopy skin

667 temperature variations in relation to climate, soil temperature, and carbon flux at a
668 ponderosa pine forest in central Oregon, *Agric. For. Meteorol.*, 226–227, 161–173,
669 doi:10.1016/j.agrformet.2016.06.001, 2016.

670 Kitz, F., Gerdel, K., Hammerle, A., Laterza, T., Spielmann, F. M. and Wohlfahrt, G.: In
671 situ soil COS exchange of a temperate mountain grassland under simulated drought,
672 *Oecologia*, 183(3), 851–860, doi:10.1007/s00442-016-3805-0, 2017.

673 Kooijmans, L. M. J. J., Maseyk, K., Seibt, U., Sun, W., Vesala, T., Mammarella, I.,
674 Kolari, P., Aalto, J., Franchin, A., Vecchi, R., Valli, G. and Chen, H.: Canopy uptake
675 dominates nighttime carbonyl sulfide fluxes in a boreal forest, *Atmos. Chem. Phys.*,
676 17(18), 11453–11465, doi:10.5194/acp-17-11453-2017, 2017.

677 Launois, T., Peylin, P., Belviso, S. and Poulter, B.: A new model of the global
678 biogeochemical cycle of carbonyl sulfide - Part 2: Use of carbonyl sulfide to constrain
679 gross primary productivity in current vegetation models, *Atmos. Chem. Phys.*, 15(16),
680 9285–9312, doi:10.5194/acp-15-9285-2015, 2015.

681 Maseyk, K., Berry, J. A., Billesbach, D., Campbell, J. E., Torn, M. S., Zahniser, M. and
682 Seibt, U.: Sources and sinks of carbonyl sulfide in an agricultural field in the Southern
683 Great Plains, *Proc. Natl. Acad. Sci.*, 111(25), 9064–9069, doi:10.1073/pnas.1319132111,
684 2014.

685 Notholt, J., Kuang, Z., Rinsland, C. P., Toon, G. C., Rex, M., Jones, N., Albrecht, T.,
686 Deckelmann, H., Krieg, J. and Weinzierl, C.: Enhanced upper tropical tropospheric COS:
687 Impact on the stratospheric aerosol layer, *Science* (80-.), 300(5617), 307–310, 2003.

688 Parker, G. G., Harmon, M. E., Lefsky, M. A., Chen, J., Pelt, R. Van, Weis, S. B.,
689 Thomas, S. C., Winner, W. E., Shaw, D. C. and Frankling, J. F.: Three-dimensional
690 Structure of an Old-growth Pseudotsuga-Tsuga Canopy and Its Implications for Radiation
691 Balance, Microclimate, and Gas Exchange, *Ecosystems*, 7(5), 440–453,
692 doi:10.1007/s10021-004-0136-5, 2004.

693 Paw U, K. T., Falk, M., Suchanek, T. H., Ustin, S. L., Chen, J., Park, Y.-S., Winner, W.
694 E., Thomas, S. C., Hsiao, T. C., Shaw, R. H., King, T. S., Pyles, R. D., Schroeder, M. and
695 Matista, A. A.: Carbon Dioxide Exchange between an Old-Growth Forest and the
696 Atmosphere, *Ecosystems*, 7(5), 513–524, doi:10.1007/s10021-004-0141-8, 2004.

697 Protoschill-Krebs, G Wilhelm, C Kesselmeier, J.: Consumption of carbonyl sulphide
698 (COS) by higher plant carbonic anhydrase (CA), *Atmos. Environ.*, 30(18), 3151–3156
699 [online] Available from:
700 <https://www.sciencedirect.com/science/article/pii/135223109600026X> (Accessed 29
701 January 2018), 1996.

702 Protoschill-Krebs, G. and Kesselmeier, J.: Enzymatic pathways for the consumption of
703 carbonyl sulphide (COS) by higher plants, *Bot. Acta*, 105, 206–212 [online] Available
704 from: <http://onlinelibrary.wiley.com/doi/10.1111/j.1438-8677.1992.tb00288.x/full>
705 (Accessed 29 January 2018), 1992.

- 706 Reichstein, M., Falge, E., Baldocchi, D., Papale, D., Aubinet, M., Berbigier, P.,
707 Bernhofer, C., Buchmann, N., Gilmanov, T. and Granier, A.: On the separation of net
708 ecosystem exchange into assimilation and ecosystem respiration: review and improved
709 algorithm, *Glob. Chang. Biol.*, 11(9), 1424–1439, 2005.
- 710 Sandoval-Soto, L., Stanimirov, M., von Hobe, M., Schmitt, V., Valdes, J., Wild, A. and
711 Kesselmeier, J.: Global uptake of carbonyl sulfide (COS) by terrestrial vegetation:
712 Estimates corrected by deposition velocities normalized to the uptake of carbon dioxide
713 (CO_2), *Biogeosciences Discuss.*, 2(1), 183–201,
714 doi:10.5194/bgd-2-183-2005, 2005.
- 715 Seibt, U., Kesselmeier, J., Sandoval-Soto, L., Kuhn, U. and Berry, J. A.: A kinetic
716 analysis of leaf uptake of COS and its relation to transpiration, photosynthesis and carbon
717 isotope fractionation, *Biogeosciences*, 7(1), 333–341, doi:10.5194/bg-7-333-2010, 2010.
- 718 Shaw, D., Franklin, J., Bible, K., Klopatek, J., Freeman, E., Greene, S. and Parker, G.:
719 Ecological Setting of the Wind River Old-growth Forest, *Ecosystems*, 7(5), 427–439,
720 doi:10.1007/s10021-004-0135-6, 2004.
- 721 Stimler, K., Nelson, D. and Yakir, D.: High precision measurements of atmospheric
722 concentrations and plant exchange rates of carbonyl sulfide using mid-IR quantum
723 cascade laser, *Glob. Chang. Biol.*, 16(9), 2496–2503, doi:10.1111/j.1365-
724 2486.2009.02088.x, 2010a.
- 725 Stimler, K., Montzka, S. A., Berry, J. A., Rudich, Y. and Yakir, D.: Relationships
726 between carbonyl sulfide (COS) and CO_2 during leaf gas exchange, *New Phytol.*, 186(4),
727 869–878, doi:10.1111/j.1469-8137.2010.03218.x, 2010b.
- 728 Sun, W., Maseyk, K., Lett, C. and Seibt, U.: Litter dominates surface fluxes of carbonyl
729 sulfide in a Californian oak woodland, *J. Geophys. Res. G Biogeosciences*, 121(2), 438–
730 450, doi:10.1002/2015JG003149, 2016.
- 731 Urban, O., Janouš, D., Acosta, M., Czerný, R., Marková, I., Navrátil, M., Pavelka, M.,
732 Pokorný, R., Šprtová, M., Zhang, R., Špunda, V. R., Grace, J. and Marek, M. V.:
733 Ecophysiological controls over the net ecosystem exchange of mountain spruce stand.
734 Comparison of the response in direct vs. diffuse solar radiation, *Glob. Chang. Biol.*,
735 13(1), 157–168, doi:10.1111/j.1365-2486.2006.01265.x, 2007.
- 736 Wehr, R., Commane, R., Munger, J. W., Barry Mcmanus, J., Nelson, D. D., Zahniser, M.
737 S., Saleska, S. R. and Wofsy, S. C.: Dynamics of canopy stomatal conductance,
738 transpiration, and evaporation in a temperate deciduous forest, validated by carbonyl
739 sulfide uptake, *Biogeosciences*, 14(2), 389–401, doi:10.5194/bg-14-389-2017, 2017.
- 740 Wharton, S. and Falk, M.: Climate indices strongly influence old-growth forest carbon
741 exchange, *Environ. Res. Lett.*, 11(4), 1–11, doi:10.1088/1748-9326/11/4/044016, 2016.
- 742 Wharton, S., Falk, M., Bible, K., Schroeder, M. and Paw U, K. T.: Old-growth CO_2 flux
743 measurements reveal high sensitivity to climate anomalies across seasonal, annual and

- 744 decadal time scales, *Agric. For. Meteorol.*, 161, 1–14,
745 doi:10.1016/j.agrformet.2012.03.007, 2012.
- 746 Whelan, M. E., Hilton, T. W., Berry, J. A., Berkelhammer, M., Desai, A. R. and
747 Campbell, J. E.: Carbonyl sulfide exchange in soils for better estimates of ecosystem
748 carbon uptake, *Atmos. Chem. Phys.*, 16(6), 3711–3726, 2016.
- 749 Whelan, M. E., Lennartz, S. T., Gimeno, T. E., Wehr, R., Wohlfahrt, G., Wang, Y.,
750 Kooijmans, L. M. J., Hilton, T. W., Belviso, S., Peylin, P., Commane, R., Sun, W., Chen,
751 H., Kuai, L., Mammarella, I., Maseyk, K., Berkelhammer, M., Li, K.-F., Yakir, D.,
752 Zumkehr, A., Katayama, Y., Ogée, J., Spielmann, F. M., Kitz, F., Rastogi, B.,
753 Kesselmeier, J., Marshall, J., Erkkilä, K.-M., Wingate, L., Meredith, L. K., He, W., Bunk,
754 R., Launois, T., Vesala, T., Schmidt, J. A., Fichot, C. G., Seibt, U., Saleska, S., Saltzman,
755 E. S., Montzka, S. A., Berry, J. A. and Campbell, J. E.: Reviews and Syntheses: Carbonyl
756 Sulfide as a Multi-scale Tracer for Carbon and Water Cycles, *Biogeosciences Discuss.*,
757 (October), 1–97, doi:10.5194/bg-2017-427, 2017.
- 758 Winner, W., Thomas, S., Berry, J., Bond, B., Cooper, C., Hinckley, T., Ehleringer, J.,
759 Fessenden, J., Lamb, B., McCarthy, S., McDowell, N., Phillips, N. and Williams, M.:
760 Canopy Carbon Gain and Water Use: Analysis of Old-growth Conifers in the Pacific
761 Northwest, *Ecosystems*, 7(5), 482–497, doi:10.1007/s10021-004-0139-2, 2004.
- 762 Wohlfahrt, G., Brilli, F., Hörtnagl, L., Xu, X., Bingemer, H., Hansel, A. and Loreto, F.:
763 Carbonyl sulfide (COS) as a tracer for canopy photosynthesis, transpiration and stomatal
764 conductance: Potential and limitations, *Plant, Cell Environ.*, 35(4), 657–667,
765 doi:10.1111/j.1365-3040.2011.02451.x, 2012.
- 766 Woodruff, D. R., McCulloh, K. A., Warren, J. M., Meinzer, F. C. and Lachenbruch, B.:
767 Impacts of tree height on leaf hydraulic architecture and stomatal control in Douglas-fir,
768 *Plant, Cell Environ.*, 30(5), 559–569, doi:10.1111/j.1365-3040.2007.01652.x, 2007.
- 769